RSC Advances

PAPER

View Article Online
View Journal | View Issue

Cite this: *RSC Adv.*, 2017, **7**, 25229

Improved Cl_2 sensing characteristics of reduced graphene oxide when decorated with copper phthalocyanine nanoflowers

Sanjeev Kumar,[a] Navdeep Kaur,[a] Anshul Kumar Sharma,[a] Aman Mahajan *[a] and R. K. Bedi[b]

Received 22nd February 2017
Accepted 5th May 2017

DOI: 10.1039/c7ra02212c

rsc.li/rsc-advances

A novel gas sensing platform involving a hybrid of reduced graphene oxide (rGO) sheets with unsubstituted copper phthalocyanine (CuPc) nanoflowers has been explored as a room temperature ppb level chemiresistive chlorine (Cl_2) sensor with a detection limit as low as 1.97 ppb. The synthesized CuPc/rGO hybrid was characterized by TEM, XRD, FTIR, Raman and UV-Vis spectroscopic and TGA techniques. Improved Cl_2 sensing characteristics of rGO on decorating with CuPc nanoflowers is attributed to the synergetic effect of the presence of more Cl_2 specific interaction sites in CuPc molecules with nanoflower type morphology along with the conducting network produced by high surface area rGO sheets. A plausible gas sensing mechanism based on Raman and electrochemical impedance spectroscopy (EIS) studies has been proposed.

1. Introduction

Cl_2 is a toxic gas with an occupational exposure limit (OEL) of 500 parts per billion (ppb) and is widely used in various industries related with pharmaceuticals, plastics, agrochemicals, water treatment, textiles and household cleaning products.[1] Cl_2 exposure above the OEL can cause a serious health risk and hence there is a need to monitor Cl_2 down to ppb range. So far, several methods like optical,[2] thermionic ionization,[3] solid state potentiometric,[4] opto-chemical,[5] calorimetric[6,7] and electrochemical[8] have been explored to detect Cl_2. These methods are complex and cumbersome. Chemiresistors on the other hand are found to be comparatively simple, economical, compact in design and consume less power. Extensive reports have been published over last few years for the detection of Cl_2 using various semiconducting oxides,[9,10] conducting polymers[11] and organic molecules[12,13] based nanostructures and thin film at room temperature.

Nowadays, the extraordinary mechanical, thermal and electrical properties of 2D monolayer of graphene with large surface area[14,15] has made it a potential candidate for detection of various toxic gases like NO_2,[16] NH_3,[17] H_2S,[18] CO_2,[19] H_2,[20] SO_2,[21] and LPG.[22] But, high cost involved in large scale production of graphene, has led to the detection of these gases using reduced graphene oxide (rGO) which is a 2D carbon based material with tuneable optical and electrical properties.[23,24] Jeong *et al.*[25] reported rGO based NO_2 gas sensor with 100 ppm detection limit, however the sensor failed to recover to original baseline on degassing. NO gas sensor with detection limit as low as 420 ppb with response time of 1000 s have been reported by Li *et al.*[26] Inkjet printed rGO based Cl_2 sensor exhibited response time of 2–3 minutes and recovery time of 2 hours with detection limit of 100 ppm.[27]

To overcome the issues of lower sensitivity, slow recovery time and detection limit in rGO based sensors, rGO has been functionalized with different metals,[28,29] metal oxides,[30–32] organic molecules[33,34] and polymers.[35,36] Such functionalization of rGO, not only improves the gas sensing parameters but also enhances their selectivity to a particular type of chemical species. Among various functionalizing species, metallophthalocyanine (MPc) based materials are demonstrated to be excellent sensing materials with high sensitivity, selectivity and fast response.[37–40]

Further, the manipulation of central metal ion, substitution of functional groups on phthalocyanine ring, morphology and operating temperature were found to remarkably tune the gas sensing characteristics of phthalocyanine molecules.[41–44] We have recently demonstrated the growth of substituted MPcs with nanowire, nanoflowers and nano belts morphology for formation of room temperature Cl_2 sensors with detection limit down to ppb level.[38–40,45] Very recently Zhao *et al.*[37] reported the growth of single crystal nano column of unsubstituted copper phthalocyanine (CuPc) for room temperature Cl_2 sensor with response of 26% for 80 ppb and Kumar *et al.*[13] reported five times enhancement in Cl_2 sensing using unsubstituted cobalt phthalocyanine (CoPc) film on porous nanostructured surface on etched glass in comparison to CoPc film on plain glass.

[a]*Material Science Laboratory, Department of Physics, Guru Nanak Dev University, Amritsar-143005, India. E-mail: aman.phy@gndu.ac.in*

[b]*Satyam Institute of Engineering and Technology, Ram Tirath Road, Amritsar-143107, India*

Functionalization of rGO with MPc molecules (MPc/rGO) has attracted remarkable attention for its distinctive selectivity toward hazardous gases due to synergetic effect of specific interaction sites in MPc molecules with conducting network provided by large surface area of rGO.[33,34] So far, Zhou *et al.*[34] have reported the functionalization of rGO with substituted metal phthalocyanine and were successful in developing room temperature sensors with a response of 15.4% for 3200 ppm of NH_3.

Herein, we report for the first time ppb level Cl_2 sensor by growing nanoflowers of CuPc molecules onto rGO sheets. The hypothesis of the work is based upon the fact that large number of gas absorbing sites provided by CuPc nanoflowers with high surface to volume ratio along with the conducting network provided by the large surface area of rGO sheets will induce selective and improved gas sensing characteristics to the hybrid.

2. Experimental details

Graphite oxide (GO) was prepared by using Hummer's method.[46] Here, 4 g of graphite flakes were treated with 2 g of $NaNO_3$ and 12 g of $KMnO_4$ in 100 ml of concentrated H_2SO_4 for the oxidation of graphite. The mixture was stirred continuously in an ice bath and H_2O was added into the obtained paste. This suspension was maintained at high temperature (98 °C) and H_2O_2 was added into the suspension for removal of impurities. The pH of solution was maintained around 7 by its several washing and filtration with warm water. Further, obtained material was centrifuged at 5500 rpm for 20 minutes and heated at 80 °C for 24 hours, thus residue as GO in powder form was collected. 10 mg of dried GO was added into 100 ml of DMF in a beaker and sonicated for exfoliating GO. Simultaneously, a solution of 0.5 mg of CuPc powder in 5 ml of DMF was prepared and added to GO solution drop by drop with continuous sonication followed by stirring in the dark for 24 hours. Thereafter, 500 μl of N_2H_4 was added in the above solution followed by refluxing at 100 °C for 24 hours. After completion of reaction, the solution was filtered and the resultant product, CuPc/rGO hybrid was dried in a vacuum oven for 3 hours at 150 °C. A schematic diagram of synthesized rGO sheets decorated with CuPc nanoflowers for chemiresistive sensor applications is depicted in Fig. 1.

The morphology of CuPc/rGO hybrid was characterized by using JEOL JEM-2100 transmission electron microscope (TEM) operating at 200 kV accelerating voltage. The structural characterization was performed using X-ray diffraction D8 FOCUS, Bruker Ettlingen (operated at 30 mA and 40 kV) with Cu K_α radiation ($\lambda = 1.5418$ Å) in the range of 5–40°. Fourier transform infrared (FTIR) spectra were recorded on Perkin Elmer Frontier instrument in the range of 400–1800 cm^{-1}. Raman spectroscopy

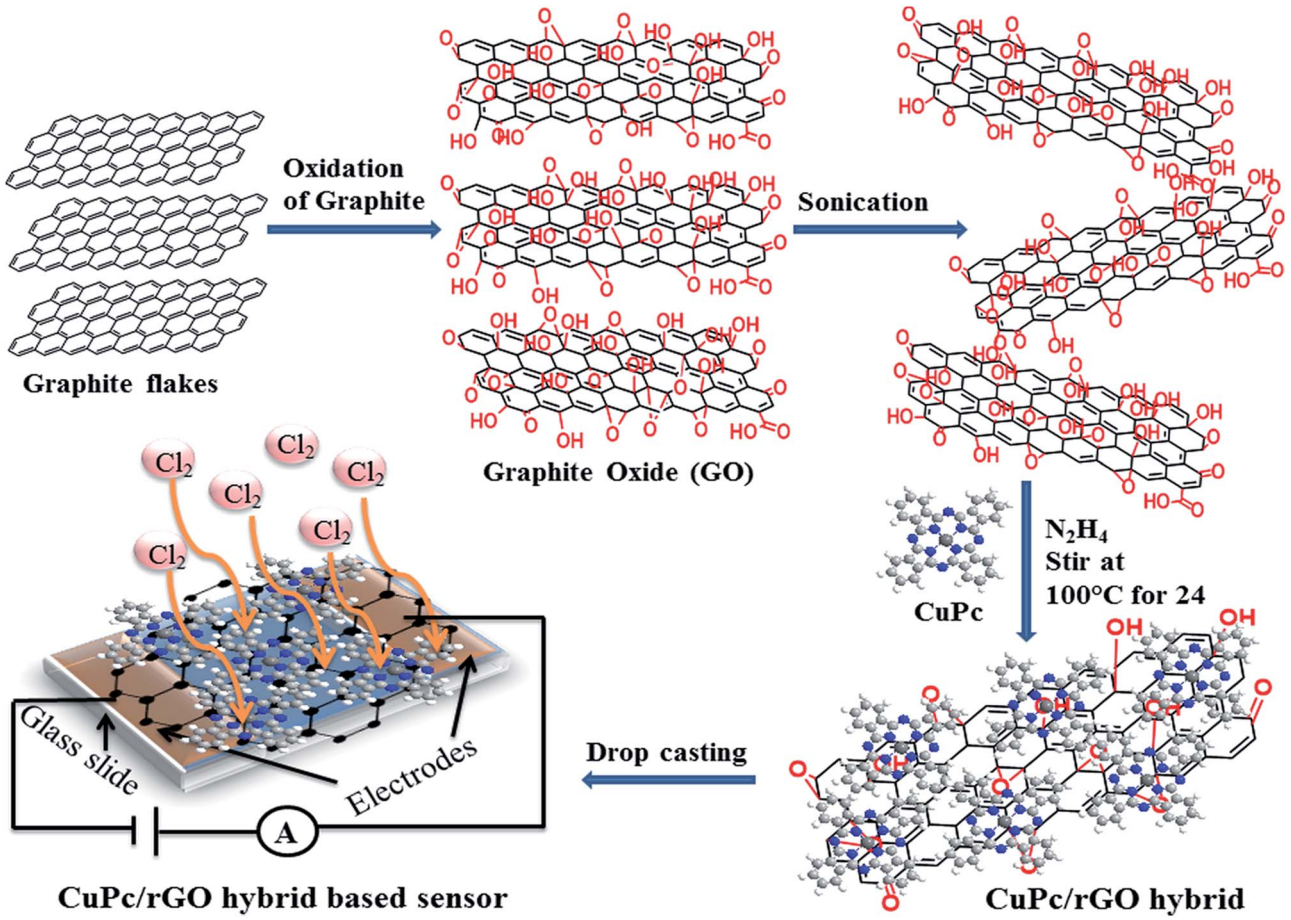

Fig. 1 Schematic diagram of synthesized rGO sheets decorated with CuPc nanoflowers for chemiresistive sensor.

was performed on Renishaw In-Via Reflex micro-Raman system from 1000 to 3200 cm^{-1} using a 514 nm argon ion laser source. UV-Vis spectroscopy was done using Shimadzu, UV-VIS-NIR 3600. Thermo gravimetric analysis (TGA) was carried out with a Thermogravimetry analyzer (Hitachi STA 7200) under a nitrogen atmosphere from 40 to 900 °C at a scan rate of 10 °C min^{-1}. Electrochemical impedance spectroscopy (EIS) was performed using a frequency response analyser (FRA) attached with Autolab potentiostat galvanostat (PGSTAT302) system. To fabricate gas sensor, two gold electrodes (50 nm thick, dimensions 5 mm × 5 mm and separated by 1 mm) were thermally deposited on glass substrate and CuPc/rGO hybrid solution of 30 μl was drop casted on it and sensor with thickness 1.2 ± 0.2 μm was obtained. The sensing studies were performed using homemade stainless steel static gas sensing instrument at room temperature (25 °C). Sensor was placed in a chamber of 1 litre volume and the temperature of the chamber was controlled by a thermocouple. The electrical conductance of the sensor was measured with Keithley electrometer (model 6517A), by applying a constant DC voltage of 3 V. Cl_2, NO_2, NO and NH_3 gases were commercially procured from Chemtron Science Pvt. Ltd., India in the gas filled canister of volume 0.5 litres with a concentration of 1000 ppm. The sensing measurement was performed by injecting a known quantity of gas using a micro-syringe. On exposure, conductance attained a maximum value and returned to base line on purging and subsequently multiple cycles of dosing and purging were performed. The response of the sensor was calculated by using equation,

$$R(\%) = \frac{C_g - C_a}{C_a} \times 100 \quad (1)$$

where C_g and C_a is the conductance of sensor in gas and in air, respectively. The response and recovery times of the hybrid were calculated as the time taken for rise and fall to 90% of the maximum value, respectively.

3. Results and discussion

3.1 Structural and spectroscopic studies

The morphology of rGO and CuPc/rGO hybrid were analysed by TEM (Fig. 2). The wrinkled and transparent sheets of rGO with folded edges are seen in Fig. 2(a). CuPc/rGO hybrid depicts the formation of uniformly grown network of nanoflowers of CuPc lying parallel to rGO surface (Fig. 2(b and c)). Fig. 3 shows the X-ray diffraction pattern of rGO, CuPc and CuPc/rGO hybrid. The rGO sample shows a diffraction peak near 25.9° which corresponds to the (002) plane. CuPc shows two diffraction peaks at 6.86° and 9.09°, corresponding to (001) and (−201) crystal planes, respectively. In Fig. 3(c), two peaks at 6.86° and 9.09° with broad spectrum at 25.9° confirms the formation of CuPc/rGO hybrid. The attachment of CuPc molecules onto rGO sheets were investigated by FTIR, Raman and UV-Vis spectroscopic studies. In FTIR spectra of rGO, peaks at 1220, 1400, 1567 and 1718 cm^{-1} corresponded to C–O–C, O–H deformation vibration, C=C and C=O stretching, respectively (Fig. 4(a)). FTIR peaks of CuPc were assigned in Fig. 4(b) and tabulated in Table 1.[47] FTIR spectra of CuPc/rGO hybrid confirmed the

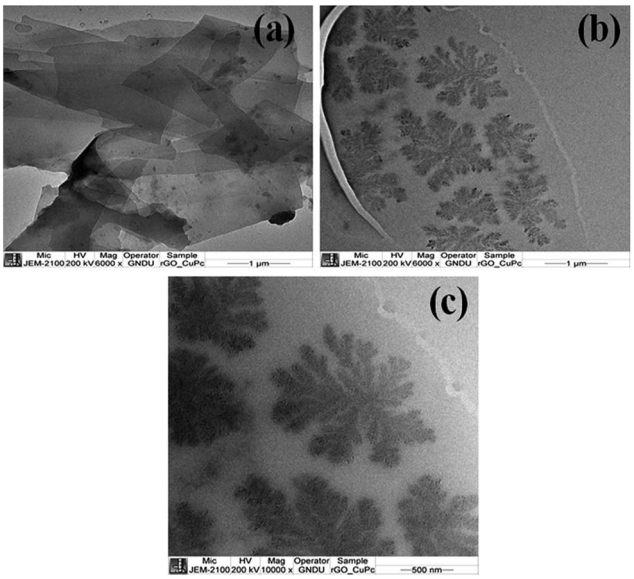

Fig. 2 TEM images of (a) rGO sheets and (b and c) CuPc nanoflowers decorated rGO sheets.

presence of all characteristic peaks of rGO and CuPc with comparatively reduced intensities. Moreover, the positions of C–O–C, C=C and C=O peaks of rGO were shifted to 1214, 1564 and 1715 cm^{-1}, respectively (Fig. 4(c)). The observed decrease in intensity and shifting of peaks after hybridization indicated the delocalization of electrons to form non-covalent attachment of CuPc on rGO surface *via* π–π interactions.[48] Raman spectra of rGO, CuPc and CuPc/rGO hybrid are shown in Fig. 5. Raman spectrum of rGO shows two characteristic G and D peaks at 1595 and 1352 cm^{-1} corresponding to the first order scattering of E_{2g} phonon of sp^2 C atoms and breathing mode of *k*-point phonons of A_{1g} symmetry (Fig. 5(a)).[11] Raman spectra of CuPc shows peaks at 594, 678, 826, 1003, 1034 and 1102 cm^{-1} corresponding

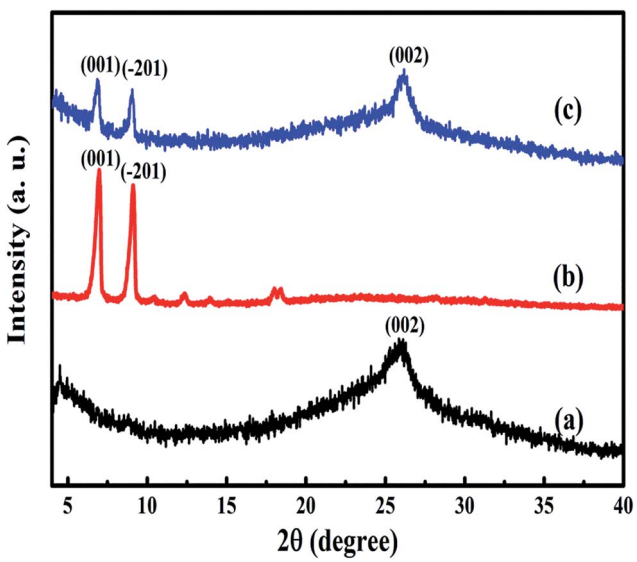

Fig. 3 XRD spectra of (a) rGO, (b) CuPc and (c) CuPc/rGO hybrid.

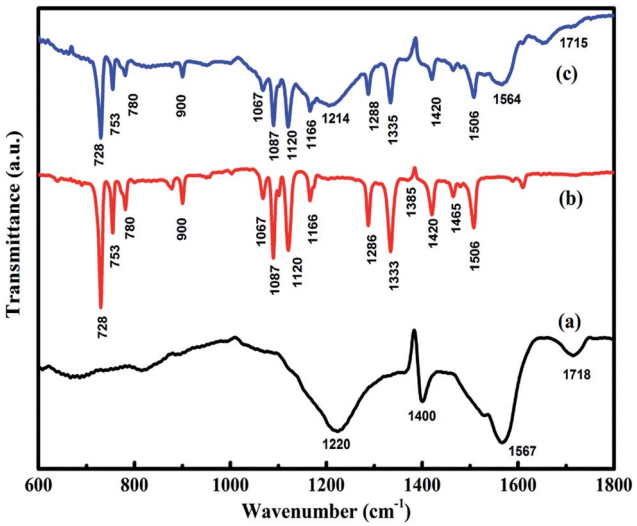

Fig. 4 FTIR spectra of (a) rGO, (b) CuPc and (c) CuPc/rGO hybrid.

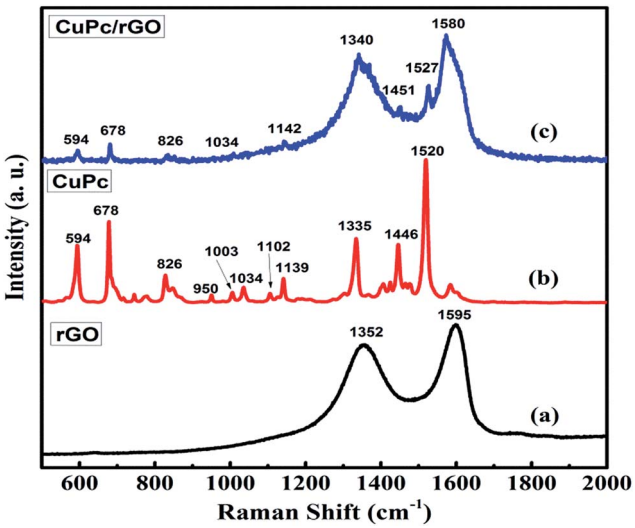

Fig. 5 Raman spectra of (a) rGO, (b) CuPc and (c) CuPc/rGO hybrid.

to A_{1g} of benzene ring deformation, B_{1g} macrocycle breathing, C–N stretching, isoindole in-plane bending, C–H bending and out of plane C–H bending, respectively. The peaks at 1335, 1446 and 1520 cm^{-1} corresponds to pyrrole stretching, isoindole ring stretching and displacement of the C–N–C bridge bond related to central copper metal ion of phthalocyanine molecule (Fig. 5(b)).[49] In the CuPc/rGO hybrid, Raman spectra peaks at 594, 678, 826, 950, 1034, 1102, 1139, 1142, 1340, 1451 and 1527 cm^{-1} corresponds to phthalocyanine molecules. The G and D peaks at 1580 and 1340 cm^{-1} shows downshift by 15 and 12 cm^{-1} in comparison to rGO spectra (Fig. 5(c)), which confirms the electron transfer interaction between the CuPc molecules and rGO sheets.[50] Further, intensity ratio (I_D/I_G) is used to identify the level of functionalization of C–C bonds. The I_D/I_G ratio of rGO and CuPc/rGO hybrid is found to be 0.86 and 1.07, respectively. The increase in I_D/I_G ratio is associated with the decrease in average size of sp^2 domains in the hybrid, caused by the non-covalent attachment of CuPc molecules onto rGO sheets.[51] Fig. 6 shows the UV-Vis spectra of rGO, CuPc and CuPc/rGO hybrid. The UV-Vis absorption spectra of rGO was found to be featureless[52] whereas CuPc exhibited three prominent absorption peaks at 362, 615 and 696 nm. The absorption peaks at 615 and 696 nm correspond to Q band of the dimer and monomer of CuPc molecules, whereas the peak at 362 nm correspond to Soret band of the phthalocyanine ring.[53] In CuPc/rGO hybrid, monomer peak of CuPc dominates over the CuPc dimer and Soret band. The monomer absorption peak was comparatively broader and red shifted by 6 nm, indicating transfer of electrons between phthalocyanine ring and rGO. This results in expanded macrocyclic conjugated structure of

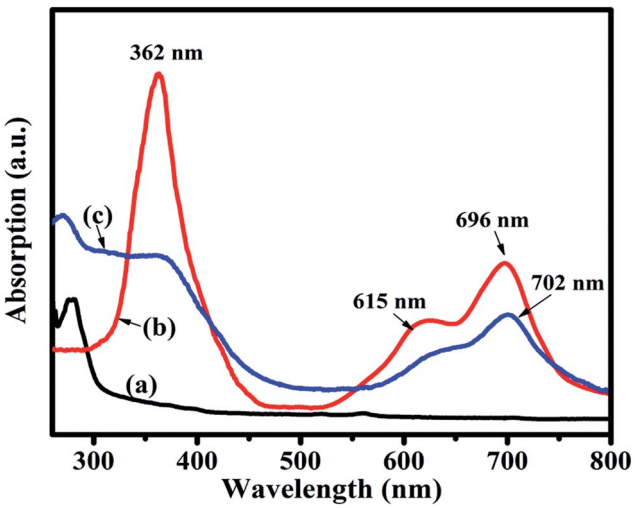

Fig. 6 UV-Vis spectra of (a) rGO, (b) CuPc and (c) CuPc/rGO hybrid.

Table 1 FTIR spectrum assignments of the CuPc

Wavenumber (cm^{-1})	Assignment	Wavenumber (cm^{-1})	Assignment
728	Out of plane C–H	1120	C–C stretching
753	Out of plane C–H deformation	1166	In plane C–N–C bending
780	Out of plane C–H deformation	1286	C–O stretching
876	Benzene wagging	1333	C–H bending
1021	Skeletal mode of central ring	1385	Isoindole stretching
1067	In plane C–H deformation	1420	In plane pyrrole stretching
1087	Cu–N stretching	1506	Pyrrole stretching

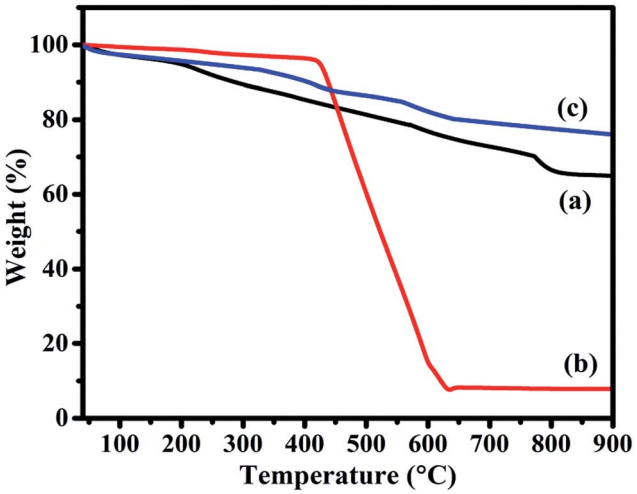

Fig. 7 TGA curve of (a) rGO, (b) CuPc and (c) CuPc/rGO hybrid under nitrogen atmosphere.

CuPc and reduced energy difference between the highest occupied molecular orbital (HOMO) and the lowest unoccupied molecular orbital (LUMO) to facilitate π–π interaction of CuPc molecule with rGO sheet.[54] In order to check the thermal stability of rGO, CuPc and CuPc/rGO hybrid, TGA was performed under a nitrogen atmosphere (Fig. 7). TGA curve of rGO shows overall weight loss of nearly 35% in the investigated temperature range (40–900 °C) and majority of weight loss is due to water adsorbents in temperature range of 70 to 180 °C. While the TGA curve of CuPc shows major weight loss from 400 to 640 °C, due to the thermal decomposition of CuPc molecules. Similarly, CuPc/rGO hybrid exhibits a weight loss of nearly 10.8% between 390 to 638 °C, due to decomposition of the CuPc on rGO surface. Further, overall weight loss of hybrid is nearly 24% in the entire investigated temperature range, suggesting that only small amount of CuPc is attached to the rGO sheets and CuPc/rGO hybrid has good thermal stability.[51,53]

3.2 Gas sensing characteristics

To study the gas sensing characteristics of CuPc/rGO hybrid sensor, we exposed the sensor to 500 ppb of Cl_2, NO_2, NO and

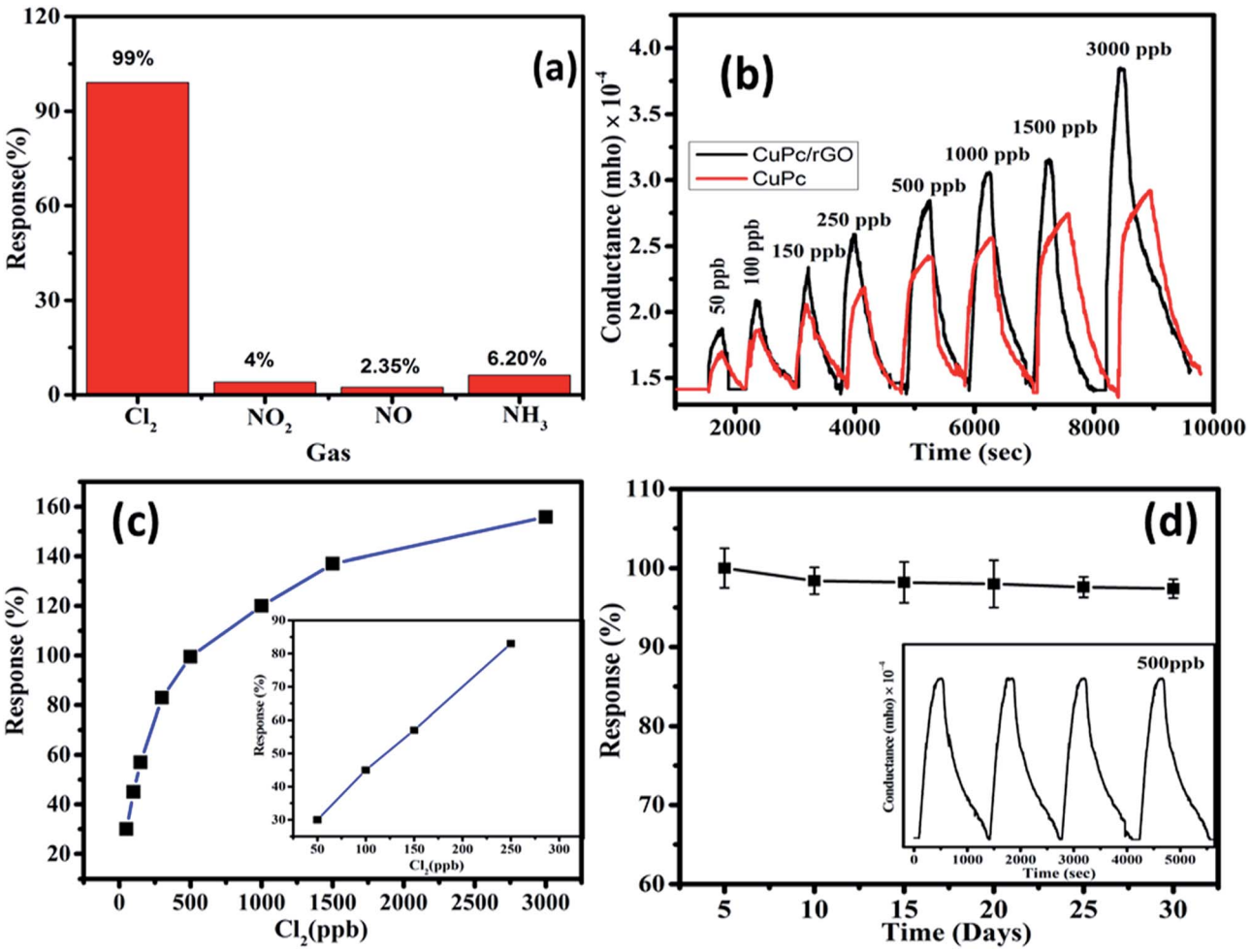

Fig. 8 (a) Response histogram of CuPc/rGO hybrid sensor to 500 ppb, (b) conductance–time plots for different doses of Cl_2, (c) variation in the response of sensor with Cl_2 concentration. The inset is a linear fitting of the response with Cl_2 concentration (d) response of the CuPc/rGO hybrid sensors to 500 ppb Cl_2 over long time storage. The inset of response curve of CuPc/rGO hybrid sensor for a repeated Cl_2 exposure of 500 ppb.

NH_3 at room temperature to check its selectivity (Fig. 8(a)). It was noted that sensor exhibited a response of 99% for Cl_2 whereas, the response for NO_2, NO and NH_3 gases were sluggish and found to be 4%, 2.35% and 6.20%, respectively. Thus, CuPc/rGO hybrid sensor is found to be highly selective towards Cl_2 as compared to other exposed gases. The conductance–time plots of CuPc and CuPc/rGO hybrid sensor for different doses of Cl_2 have been shown in Fig. 8(b). It demonstrates that there was an increase in the sensor conductance after exposure to Cl_2 and it gets saturated after some time and after purging air, sensor conductance reaches to its original baseline, thus showing good reversibility of sensor. While in case of CuPc sensor, the sensor response is lesser in comparison to CuPc/rGO hybrid sensor. For 3000 ppb of Cl_2, hybrid sensor exhibits response as large as 156% with a response/recovery time of 190/545 s, respectively. The faster response time, reversible and reproducible response is due to large number of Cl_2 selective sensing sites provided by CuPc nanoflowers which are further non-covalently attached to large surface area rGO sheets in CuPc/rGO hybrid. Fig. 8(c) shows that the response of hybrid sensor increases from 30% to 156% with an increase in Cl_2 concentration (50–3000 ppb). The linear region observed in lower concentration range (50–250 ppb) has been shown in the inset of Fig. 8(c). This behaviour can be understood on the basis of effective occupancy of active sites. As seen from TEM images of the hybrid, nanoflower structures of CuPc molecules onto rGO sheets provide large number of active sites. At low concentration, abundant active sites are available and response increases with increase in concentration. To check the reproducibility of the response, CuPc/rGO sensor is repeatedly exposed to 500 ppb of Cl_2 at room temperature and it is observed that response of sensor remains nearly same (inset of Fig. 8(d)) without any drift in the baseline conductance and hence sensor is reproducible. We have also investigated the repeatability and stability of CuPc/rGO hybrid sensor devices. Out of different fabricated sensors, set of randomly selected five sensors were checked for Cl_2 sensing at room temperature. A small deviation in sensor response from its average value indicates high degree of repeatability of fabricated devices. The response of the sensors remains almost same even after 30 days (Fig. 8(d)), which depicts that the sensors have a long-term stability.

The lowest detectable concentration, being reported here, is dependent on the experimental set up used. However, the minimum detection limit of sensor can be calculable from signal to noise ratio (S/N) using the formula,[55,56]

$$\text{Detection limit} = 3 \times \frac{\text{concentration}}{\text{S/N}}$$

where S is $C_g - C_a$ and N is the conductance base line noise before gas exposure. The detection limit of CuPc/rGO hybrid sensor at room temperature is found to be 1.97 ppb. Thus, the faster response time, reversible and reproducible Cl_2 sensing characteristics of the CuPc/rGO sensor along with low detection limit in comparison to other rGO and CuPc based Cl_2 sensor reported in literature[27,37] makes it a promising candidate for ppb level Cl_2 detection.

3.3 Gas sensing mechanism

The underlying mechanism of CuPc/rGO hybrid sensor for Cl_2 has been investigated using Raman and EIS. Raman spectra of CuPc/rGO hybrid sensor with exposure to 1000 ppb of Cl_2 (Fig. 9) shows a change in position and intensity of peaks w.r.t. unexposed sensor. The peaks at 594, 678, 831 and 1143 cm^{-1} corresponding to the region of macrocyclic vibrations of CuPc molecules[45,55] shows a downshift of 2 cm^{-1} on Cl_2 exposure (Fig. 9(b)). A significant shift of 5 and 6 cm^{-1} is observed in the peaks at 1451 and 1527 cm^{-1} corresponding to isoindole ring vibration and displacement of the C–N–C bridge bond related to central copper metal ions.[56] This confirms that interaction of Cl_2 most probably occurs at copper metal ions of CuPc/rGO hybrid. After purging air, peaks again recover to their original position indicating reversibility of fabricated sensor (Fig. 9(c)). EIS has been used to understand the contributions of bulk resistance of rGO sheets (R_0), resistance and capacitance across the grain boundaries between CuPc/rGO grains (R_1 and C_1), contact resistance and capacitance between hybrid and metal electrode (R_2 and C_2) towards sensor response. Fig. 10(A) shows the Nyquist plot of CuPc/rGO hybrid plotted between real component (Z' (Ω)) and imaginary component ($-Z''$ (Ω)) from low (0.1 Hz) to high frequency (1 MHz). The impedance measurement has been carried out in the presence of air and after exposure to 1000 ppb of Cl_2. A single semicircle is observed before and after exposure to Cl_2 and is fitted (solid line) using equivalent circuit consisting of R_0 in series with two RC networks as shown in Fig. 10(B). It is observed that, after exposure of Cl_2 the diameter of semicircle is reduced leading to decrease in R_0, R_1 and R_2 and corresponding increase in C_1 and C_2 in comparison to unexposed Cl_2 (Table 2). The prominent change in R_1 and C_1 suggests that incoming Cl_2 gas molecules physiosorbed onto grain boundaries separating grains of CuPc

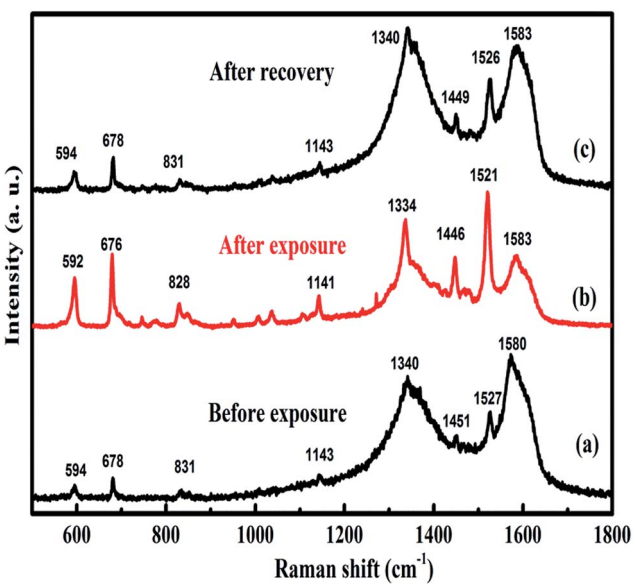

Fig. 9 Raman spectra of CuPc/rGO hybrid recorded (a) before exposure, (b) after exposure and (c) after recovery to 1000 ppb of Cl_2.

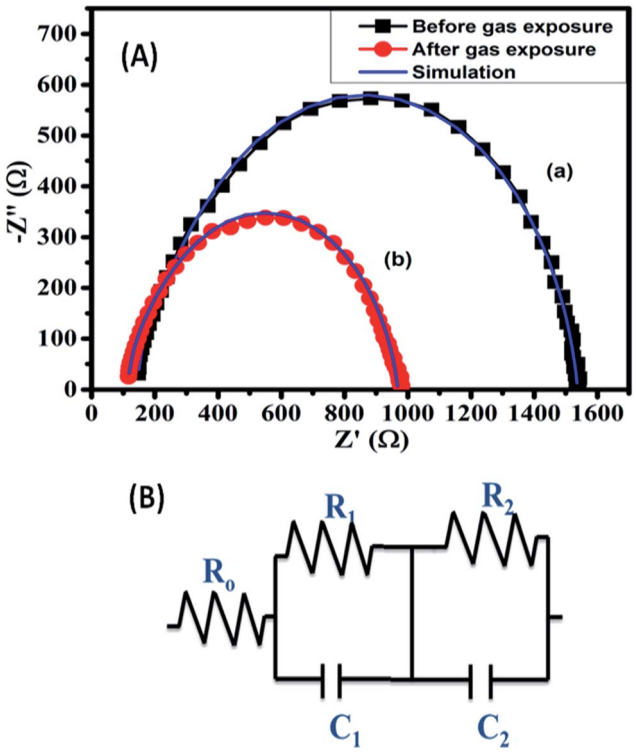

Fig. 10 (A) Impedance spectra of CuPc/rGO hybrid (a) before and (b) after exposure to 1000 ppb of Cl_2 and (B) equivalent circuit to interpret the impedance spectroscopy data.

Table 2 Impedance parameters obtained for CuPc/rGO hybrid by fitting experimental curve to the equivalent circuit

	R_0 (Ω)	R_1 (Ω)	R_2 (Ω)	C_1 (nF)	C_2 (nF)
Unexposed gas	149	1150	216	9.78	7.71
Exposed gas	119	653	180	13.5	9.16

molecules and rGO sheets, which are the dominating sites for physio-sorption. This physio-sorption improves conductivity of the sensor through electron charge transfer from CuPc to rGO sheets, which acts as the conducting network between them.

4. Conclusions

We have demonstrated that small organic semiconducting molecules with controlled nanostructured morphology on combining with conducting platform can be utilized as selective and highly sensitive sensor. The illustration has been made by combining the properties of CuPc and rGO to produce Cl_2 selective room temperature chemiresistor with minimum detection limit of 1.97 ppb. Structural and spectroscopic studies confirmed that CuPc nanoflower structures are non-covalently attached on rGO sheets. The physio-sorption of incoming Cl_2 molecules on central metal ion present on the grains of CuPc decorated rGO sheets is responsible for selective Cl_2 detection. Moreover, nanoflower morphology of CuPc provides large number of physio-sorption sites and conducting network of large surface area of rGO sheets improve the Cl_2 sensing of present sensor.

Acknowledgements

The authors would like to acknowledge DAE-BRNS, Mumbai, India for providing financial assistance to carry out this research work. One of the authors, Sanjeev Kumar is grateful to UGC-RGNF New Delhi, India for awarding senior research fellowship.

References

1 A. K. Saroha, *J. Chem. Health Saf.*, 2006, **13**, 5–11.
2 S. Usha, S. Mishra and B. Gupta, *Materials*, 2015, **8**, 2204.
3 C. F. Poole, *J. Chromatogr. A*, 2015, **1421**, 137–153.
4 H. Zhang, J. Li, H. Zhang, X. Liang, C. Yin, Q. Diao, J. Zheng and G. Lu, *Sens. Actuators, B*, 2013, **180**, 66–70.
5 M. Ralfs and J. Heinze, *Sens. Actuators, B*, 1997, **44**, 257–261.
6 L. Huixia, L. Yong, T. Yanni, L. Lanlan, Z. Qing, L. Kun and T. Hanchun, *New J. Chem.*, 2015, **39**, 3865–3874.
7 Y. Xiong, J. Tan, C. Wang, J. Wu, Q. Wang, J. Chen, S. Fang and M. Duan, *Sens. Actuators, B*, 2017, **245**, 674–682.
8 K. Senthilkumar and J.-M. Zen, *Electrochem. Commun.*, 2014, **46**, 87–90.
9 S. M. Ingole, S. T. Navale, Y. H. Navale, D. K. Bandgar, F. J. Stadler, R. S. Mane, N. S. Ramgir, S. K. Gupta, D. K. Aswal and V. B. Patil, *J. Colloid Interface Sci.*, 2017, **493**, 162–170.
10 S. T. Navale, V. V. Jadhav, K. K. Tehare, R. U. R. Sagar, C. S. Biswas, M. Galluzzi, W. Liang, V. B. Patil, R. S. Mane and F. J. Stadler, *Sens. Actuators, B*, 2017, **238**, 1102–1110.
11 D. R. Kumar, S. Kesavan, T. T. Nguyen, J. Hwang, C. Lamiel and J.-J. Shim, *Sens. Actuators, B*, 2017, **240**, 818–828.
12 A. Singh, A. Kumar, A. Kumar, S. Samanta, N. Joshi, V. Balouria, A. K. Debnath, R. Prasad, Z. Salmi, M. M. Chehimi, D. K. Aswal and S. K. Gupta, *Appl. Phys. Lett.*, 2013, **102**, 132107.
13 A. Kumar, S. Samanta, S. Latha, A. K. Debnath, A. Singh, K. P. Muthe and H. C. Barshilia, *RSC Adv.*, 2017, **7**, 4135–4143.
14 A. K. Geim and K. S. Novoselov, *Nat. Mater.*, 2007, **6**, 183–191.
15 K. S. Novoselov, A. K. Geim, S. V. Morozov, D. Jiang, Y. Zhang, S. V. Dubonos, I. V. Grigorieva and A. A. Firsov, *Science*, 2004, **306**, 666–669.
16 F. Yavari, E. Castillo, H. Gullapalli, P. M. Ajayan and N. Koratkar, *Appl. Phys. Lett.*, 2012, **100**, 203120.
17 M. Gautam and A. H. Jayatissa, *J. Appl. Phys.*, 2012, **112**, 064304.
18 B. Paulus and K. Rosciszewski, *Int. J. Quantum Chem.*, 2009, **109**, 3055–3062.
19 H. J. Yoon, D. H. Jun, J. H. Yang, Z. Zhou, S. S. Yang and M. M.-C. Cheng, *Sens. Actuators, B*, 2011, **157**, 310–313.
20 R. C. Ehemann, P. S. Krstić, J. Dadras, P. R. Kent and J. Jakowski, *Nanoscale Res. Lett.*, 2012, **7**, 198.
21 Y. Ren, C. Zhu, W. Cai, H. Li, H. Ji, I. Kholmanov, Y. Wu, R. D. Piner and R. S. Ruoff, *Appl. Phys. Lett.*, 2012, **100**, 163114.

22 K. R. Nemade and S. A. Waghuley, *J. Electron. Mater.*, 2013, **42**, 2857–2866.
23 L. Ganhua, E. O. Leonidas and C. Junhong, *Nanotechnology*, 2009, **20**, 445502.
24 R. K. Joshi, H. Gomez, F. Alvi and A. Kumar, *J. Phys. Chem. C*, 2010, **114**, 6610–6613.
25 H. Y. Jeong, D.-S. Lee, H. K. Choi, D. H. Lee, J.-E. Kim, J. Y. Lee, W. J. Lee, S. O. Kim and S.-Y. Choi, *Appl. Phys. Lett.*, 2010, **96**, 213105.
26 W. Li, X. Geng, Y. Guo, J. Rong, Y. Gong, L. Wu, X. Zhang, P. Li, J. Xu, G. Cheng, M. Sun and L. Liu, *ACS Nano*, 2011, **5**, 6955–6961.
27 V. Dua, S. P. Surwade, S. Ammu, S. R. Agnihotra, S. Jain, K. E. Roberts, S. Park, R. S. Ruoff and S. K. Manohar, *Angew. Chem., Int. Ed. Engl.*, 2010, **49**, 2154–2157.
28 L. Huang, Z. Wang, J. Zhang, J. Pu, Y. Lin, S. Xu, L. Shen, Q. Chen and W. Shi, *ACS Appl. Mater. Interfaces*, 2014, **6**, 7426–7433.
29 R. Furue, E. P. Koveke, S. Sugimoto, Y. Shudo, S. Hayami, S.-I. Ohira and K. Toda, *Sens. Actuators, B*, 2017, **240**, 657–663.
30 Q. Feng, X. Li, J. Wang and A. M. Gaskov, *Sens. Actuators, B*, 2016, **222**, 864–870.
31 U. Yaqoob, A. S. M. I. Uddin and G.-S. Chung, *Sens. Actuators, B*, 2016, **224**, 738–746.
32 S. Liu, Z. Wang, Y. Zhang, C. Zhang and T. Zhang, *Sens. Actuators, B*, 2015, **211**, 318–324.
33 X. Li, B. Wang, X. Wang, X. Zhou, Z. Chen, C. He, Z. Yu and Y. Wu, *Nanoscale Res. Lett.*, 2015, **10**, 373.
34 X. Zhou, X. Wang, B. Wang, Z. Chen, C. He and Y. Wu, *Sens. Actuators, B*, 2014, **193**, 340–348.
35 L. Al-Mashat, K. Shin, K. Kalantar-zadeh, J. D. Plessis, S. H. Han, R. W. Kojima, R. B. Kaner, D. Li, X. Gou, S. J. Ippolito and W. Wlodarski, *J. Phys. Chem. C*, 2010, **114**, 16168–16173.
36 Y. Zhao, X.-g. Li, X. Zhou and Y.-n. Zhang, *Sens. Actuators, B*, 2016, **231**, 324–340.
37 J. Zhao, Z. Qiao, Y. Zhang, T. Zou, L. Yu, L. Luo, X. Wang, Y. Yang, H. Wang and L. Tang, *AIP Adv.*, 2016, **6**, 095303.
38 R. Saini, A. Mahajan, R. K. Bedi, D. K. Aswal and A. K. Debnath, *Sens. Actuators, B*, 2014, **203**, 17–24.
39 R. Saini, A. Mahajan, R. K. Bedi, D. K. Aswal and A. K. Debnath, *Sens. Actuators, B*, 2014, **198**, 164–172.
40 R. Saini, A. Mahajan, R. K. Bedi, D. K. Aswal and A. K. Debnath, *RSC Adv.*, 2014, **4**, 15945–15951.
41 F. I. Bohrer, C. N. Colesniuc, J. Park, M. E. Ruidiaz, I. K. Schuller, A. C. Kummel and W. C. Trogler, *J. Am. Chem. Soc.*, 2009, **131**, 478–485.
42 R. D. Yang, J. Park, C. N. Colesniuc, I. K. Schuller, J. E. Royer, W. C. Trogler and A. C. Kummel, *J. Chem. Phys.*, 2009, **130**, 164703.
43 X. Ding, H. Xu, L. Zhang, D. Jiang and A. Lu, *Mol. Cryst. Liq. Cryst. Sci. Technol., Sect. A*, 1999, **337**, 481–484.
44 B. Wang, X. Zhou, Y. Wu, Z. Chen, C. He and X. Zuo, *Sens. Actuators, B*, 2012, **161**, 498–503.
45 G. S. S. Saini, S. Sukhwinder, K. Sarvpreet, K. Ranjan, S. Vasant and S. K. Tripathi, *J. Phys.: Condens. Matter*, 2009, **21**, 225006.
46 W. S. Hummers and R. E. Offeman, *J. Am. Chem. Soc.*, 1958, **80**, 1339.
47 T. V. Basova, I. V. Jushina, A. G. Gürek, D. Atilla and V. Ahsen, *Dyes Pigm.*, 2009, **80**, 67–72.
48 B. Wang, Y. Wu, X. Wang, Z. Chen and C. He, *Sens. Actuators, B*, 2014, **190**, 157–164.
49 R. Prabakaran, R. Kesavamoorthy, G. L. N. Reddy and F. P. Xavier, *Phys. Status Solidi B*, 2002, **229**, 1175–1186.
50 A. Chunder, T. Pal, S. I. Khondaker and L. Zhai, *J. Phys. Chem. C*, 2010, **114**, 15129–15135.
51 J.-P. Zhong, Y.-J. Fan, H. Wang, R.-X. Wang, L.-L. Fan, X.-C. Shen and Z.-J. Shi, *J. Power Sources*, 2013, **242**, 208–215.
52 H. Zhao, Y. Zhang, B. Zhao, Y. Chang and Z. Li, *Environ. Sci. Technol.*, 2012, **46**, 5198–5204.
53 B.-P. Jiang, L.-F. Hu, D.-J. Wang, S.-C. Ji, X.-C. Shen and H. Liang, *J. Mater. Chem. B*, 2014, **2**, 7141–7148.
54 S. A. Mamuru, K. I. Ozoemena, T. Fukuda, N. Kobayashi and T. Nyokong, *Electrochim. Acta*, 2010, **55**, 6367–6375.
55 L. L. Gladkov, V. V. Gromak and V. K. Konstantinova, *J. Appl. Spectrosc.*, 2007, **74**, 328–332.
56 M. Szybowicz and J. Makowiecki, *J. Mater. Sci.*, 2012, **47**, 1522–1530.